DOI:
10.1103/PhysRevB.91.195411

Document Version
Publisher's PDF, also known as Version of record

Effect of disorder on Raman scattering of single-layer MoS_2

Sandro Mignuzzi,[1,2,*] Andrew J. Pollard,[1] Nicola Bonini,[2] Barry Brennan,[1] Ian S. Gilmore,[1] Marcos A. Pimenta,[3] David Richards,[2] and Debdulal Roy[1,†]

[1]*National Physical Laboratory, Hampton Road, Teddington TW11 0LW, United Kingdom*

[2]*Department of Physics, King's College London, Strand, London WC2R 2LS, United Kingdom*

[3]*Departamento de Física, Universidade Federal de Minas Gerais, Caixa Postal 702, 30123-970 Belo Horizonte, Brazil*

(Received 26 January 2015; published 11 May 2015)

We determine the effect of defects induced by ion bombardment on the Raman spectrum of single-layer molybdenum disulfide. The evolution of both the linewidths and frequency shifts of the first-order Raman bands with the density of defects is explained with a phonon confinement model, using density functional theory to calculate the phonon dispersion curves. We identify several defect-induced Raman scattering peaks arising from zone-edge phonon modes. Among these, the most prominent is the LA(M) peak at $\sim$227 cm^{-1} and its intensity, relative to the one of first-order Raman bands, is found to be proportional to the density of defects. These results provide a practical route to quantify defects in single-layer MoS_2 using Raman spectroscopy and highlight an analogy between the LA(M) peak in MoS_2 and the D peak in graphene.

DOI: 10.1103/PhysRevB.91.195411 PACS number(s): 61.72.Dd, 78.30.Ly, 61.80.Jh, 71.15.Mb

I. INTRODUCTION

The considerable research interest in atomically thin graphene over the last decade has paved the way for the investigation of many other two-dimensional (2D) materials [1]. Among these, semiconducting single-layer molybdenum disulfide (1L-MoS_2) shows technologically exploitable electronic [2,3] and optical [2,4] properties, and is a promising candidate as a building block in functional heterostructures [1].

The performance of MoS_2-based devices is expected to be critically affected by structural disorder, which may be induced during synthesis or processing. However, the controlled introduction of defects can also be utilized to tailor the properties of 1L-MoS_2, for example: line defects in 1L-MoS_2 can act as one-dimensional (1D) metallic stripes [5]; the introduction of vacancies, using electron irradiation can lead to the doping of 1L-MoS_2 [6] and enhance its photoluminescence [7]; the reactivity of MoS_2 can be improved in the presence of structural defects or by increasing active edge sites, making its amorphous phase interesting for electrocatalysis applications [8]; ion irradiation can be used to thin MoS_2 down to single layers and to engineer the properties of MoS_2-based devices [9]. Therefore, investigating the fundamental physics, and quantifying the level of disorder in this material are key steps towards the large-scale synthesis of 1L-MoS_2 and also subsequent device fabrication and material functionalization.

Raman spectroscopy is a widely established technique that can be used to gain insight into the vibrational properties of MoS_2 as well as the perturbation of its crystal lattice, induced by doping [10] or strain [11]. The Raman spectrum of bulk MoS_2 is characterized by two prominent peaks denoted as E^1_{2g} ($\sim$382 cm^{-1}) and A_{1g} ($\sim$407 cm^{-1}); these are the first-order Raman modes associated with in-plane and out-of-plane vibrations, respectively. When the thickness of MoS_2 decreases, the frequency of E^1_{2g} upshifts while the frequency of A_{1g} downshifts, until a frequency difference of $\sim$19 cm^{-1} between the two peaks is reached for 1L-MoS_2, allowing identification of the number (N) of layers [12]. Strictly speaking, due to the different symmetries between odd and even N, one should refer to these peaks as E^1_{2g} and A_{1g} for even N only, and to E' and A'_1 for odd N [13]. The latter notation will be used throughout this report, as it applies to 1L-MoS_2.

In this article we report a Raman spectroscopy study of defective 1L-MoS_2. Ion bombardment is used as a method to introduce defects in 1L-MoS_2, specifically, a manganese ion (Mn^+) gun to provide nanometer-sized defects [14], with a controllable defect density [14–17]. The introduction of structural disorder results in the observation of specific Raman signatures, thus indicating the viability of Raman spectroscopy as a high-throughput and nondestructive technique to quantify defects in 1L-MoS_2.

II. METHODS

Using micromechanical cleavage [18], natural bulk MoS_2 is exfoliated and deposited on Si substrates covered with 300 nm SiO_2. Photoluminescence [4] and Raman spectroscopy [12] are used to unambiguously identify 1L-MoS_2 flakes. The 1L-MoS_2 flakes are bombarded with Mn^+, each with a different ion dose, in an ultrahigh vacuum (UHV) time-of-flight secondary ion mass spectrometry (TOF-SIMS IV) instrument (ION-TOF GmbH, Muenster, Germany), equipped with a liquid metal ion gun at an angle of 45° to the surface normal and using an ion-beam kinetic energy of 25 keV. Each 1L-MoS_2 flake is on a different Si substrate and is dosed during different experiments, in order to verify the reproducibility of the results. Defects are created in 1L-MoS_2 flakes by single ion impact events and, in order to induce a controllable and quantifiable level of surface damage, the ion beam is rastered over the 1L-MoS_2 surface. The density of ions impinging on the surface (σ) is calculated as $\sigma = it/Ae$, where i is the ion current, t is the exposure time to the ion beam, A is the rastered area, and e is the elementary charge. By varying t it is possible to tune the defect density between 10^{12} and

*sandro.mignuzzi@kcl.ac.uk
†debdulal.roy@npl.co.uk

10^{14} ions/cm^2. These correspond to an average interdefect distance (L_D) ranging from 10 to 1 nm ($L_D = 1/\sqrt{\sigma}$). The ion beam has a Gaussian distribution with a full width at half maximum of approximately 4 μm and is digitally rastered over a square area of side between 100 and 200 μm. Consequently, from the single ion impact statistics alone, the ion dose distribution is uniform to better than 99.9999% within 20 μm of the ion bombarded perimeter (5 standard deviations of the ion beam). Since the average interdefect distance is inversely proportional to the square root of the ion dose density, there is a high degree of uniformity over this central region where the 1L-MoS_2 flake is located. In practice the uniformity is reduced since the ion beam current, measured using a Faraday cup, has a small variation (standard deviation of up to 1%), which is reflected as the uncertainty in the interdefect distance. Raman spectra are collected at room temperature, in ambient conditions, on both the pristine and bombarded flakes, using a confocal system (LabRAM HR800, Horiba Jobin Yvon) in backscattering geometry, equipped with a 100× objective (numerical aperture NA = 0.9) and a 600 lines/mm grating. The spectral resolution is ~2 cm^{-1}, as derived from the linewidth of the Rayleigh peak, with an uncertainty in the Raman shift position of ±1 cm^{-1} due to instrumentation. Measurements are performed using a green (532 nm) laser excitation wavelength. The laser power is kept below 100 μW to avoid heating effects and thermal damage. The Si Raman band at 520 cm^{-1} is used as a reference for the calibration of the Raman shift. The phonon frequencies of 1L-MoS_2 are computed using density functional theory (DFT) and density-functional perturbation theory as implemented in the QUANTUM-ESPRESSO distribution [19], within the local density approximation [20], using norm-conserving pseudopotentials. A plane-wave expansion up to a 90 Ry cutoff is used and the Brillouin zone is sampled with a 12×12×1 Monkhorst-Pack mesh. The 1L-MoS_2 is modeled using a supercell approach and an interlayer spacing of 1.0 nm. The dynamical matrices are calculated on an 8×8×1 uniform mesh and Fourier interpolation is used to compute the phonon dispersion on finer grids.

III. RESULTS AND DISCUSSION

Figure 1 shows the development of representative Raman spectra of 1L-MoS_2 flakes, bombarded with Mn^+, for an increasing density of defects. The bottom Raman spectrum of Fig. 1 is for a pristine flake and shown for comparison. Notably, as observed in Fig. 1, the Raman spectrum gradually evolves as a function of L_D. This evolution can be summarized in two main points: (i) the first-order Raman bands show changes in both their widths and positions, and (ii) new Raman scattering peaks arise in the spectral region ~140–420 cm^{-1}.

Focusing our attention on the two main first-order Raman bands (Fig. 2), as L_D decreases we observe that the peak position of E', Pos(E'), downshifts while that of A'_1, Pos(A'_1), upshifts, whereas the full width at half maxima Γ of both bands, Γ(E') and Γ(A'_1), increase upon decreasing L_D. In order to exclude any possible contribution of temperature-induced broadening and shifts of the Raman scattering peaks, we measured the Raman spectra as a function of laser power, confirming that no significant variation is found in the

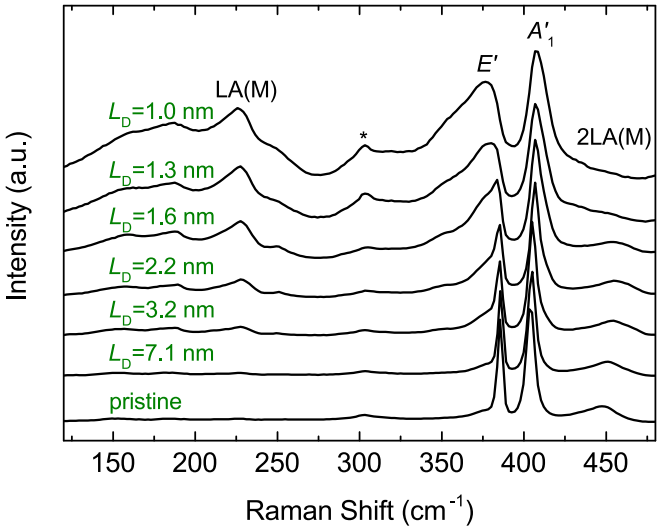

FIG. 1. (Color online) Raman spectra of 1L-MoS_2 flakes with varying interdefect distances L_D. The asterisk refers to the 2TA(X) Raman peak of the Si substrate. The spectra have been normalized to the intensity of the A'_1 peak, as seen from the relative increase of 2TA(X) with decreasing L_D.

Raman spectra for the laser power range 1 μW–1 mW (see Supplemental Material [21]). We note that ion-induced defects in 2D materials are usually associated with doping [22] and strain [23], which can affect the vibrational modes. Indeed, it has been previously observed that Pos(A'_1) and Γ(A'_1) are sensitive to doping, whereas E' remains unaffected [10]. However, the upshift of Pos(A'_1) should be accompanied by a decrease of Γ(A'_1) [10], which is inconsistent with our observation, allowing us to rule out the doping effect as the main mechanism involved. One could also associate the shift in peaks position with an induced strain localized around defects. It has indeed been reported that both Pos(E') and Pos(A'_1) decrease (increase) with tensile (compressive) in-plane strain [11,24], which is once again contrary to our experimental observations. However, although doping and strain will have an effect on the Raman spectra, the observed disorder-related evolution of the first-order peaks can instead be explained using a "phonon confinement model," as reported for ion-bombarded graphene [16] and other disordered crystals [25–27].

For a crystalline material, the vibrational normal modes have an infinite spatial correlation. Therefore, Raman active phonons can be described as plane waves with finite wave vector $\mathbf{q} \cong 0$ (known as the Raman fundamental selection rule). The corresponding Raman bands have Lorentzian line shapes centered at frequency ω of the zone center of the Brillouin zone, with a full width at half maximum, Γ_0, which is inversely proportional to the phonon lifetime. When defects are introduced, these perturb the spatial translational invariance of the system; as a consequence, the phonon correlation length L_C becomes finite, causing the breakdown of the fundamental selection rule [27]. The relaxation of the selection rule determined by the presence of disorder can be taken into account by considering an "effective" circular region, with diameter equal to L_C, within which the phonons are confined,

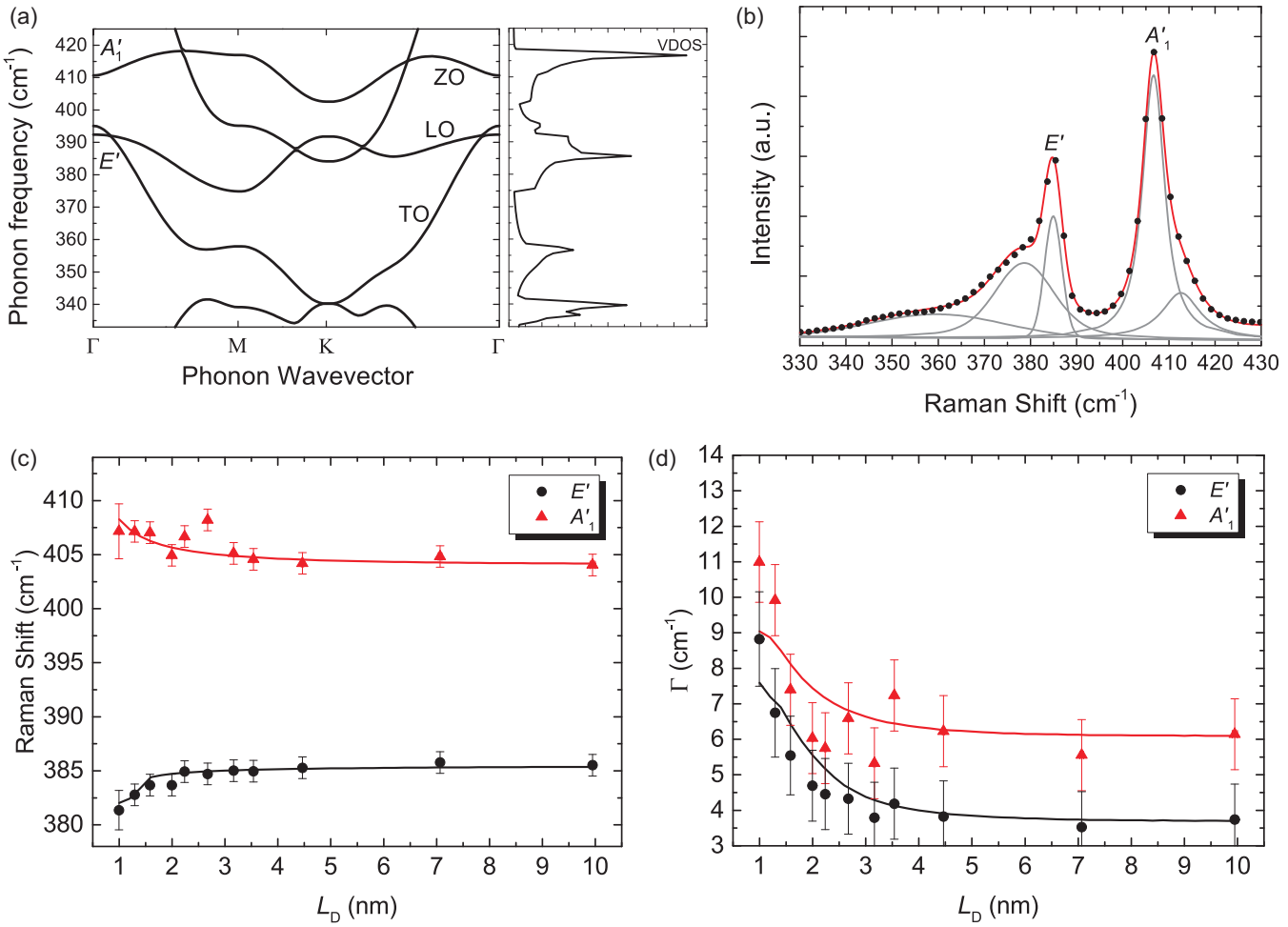

FIG. 2. (Color online) (a) Phonon dispersion and vibrational density of states of 1L-MoS_2. (b) Close-up of the spectral region where the first-order peaks are located, for sample with $L_D = 2.2$ nm. The gray lines are the fitted Voigt peaks, and the red line is the cumulative spectrum from the Voigt fitting process. Symbols represent the experimental spectrum. (c) Position and (d) Γ of E' and A'_1 as a function of L_D. Symbols refer to experimental data, continuous lines refer to the phonon confinement model described in the main text. The error bars for the peak position and Γ represent the largest uncertainty present (the spectrometer resolution or the standard error from the fitting process).

leading to a Gaussian attenuation factor of $\exp(-2r^2/{L_C}^2)$, where r is the spatial coordinate. In the reciprocal lattice space, this corresponds to a phonon wave packet of $\exp(-q^2{L_C}^2/4)$. As a consequence, the intensity I of a Raman band can be generalized as

$$I(\omega) = \int_{BZ} \frac{\exp\left(-\frac{\mathbf{q}^2 L_C^2}{4}\right)}{[\omega - \omega(\mathbf{q})]^2 + \left(\frac{\Gamma_0}{2}\right)^2} d^2\mathbf{q}, \qquad (1)$$

where $\omega(\mathbf{q})$ is the phonon dispersion and the integral is extended over the Brillouin zone. For pristine materials, L_C tends to infinity and Eq. (1) reduces to a single Lorentzian centered at $\omega(0)$. This Raman line-shape interpretation, which is known in literature as "phonon confinement model" or "spatial correlation model," has been successfully applied to explain the Raman scattering from several ion-bombarded crystals, for example, graphene [16], graphite [25], and GaAs [26], as well as to estimate the domain size of microcrystalline silicon [27,28] and the width of silicon nanowires [29].

In this work we model the line shapes of the first-order peaks using Eq. (1), where Γ_0 is taken as the experimental width of each Raman scattering peak, as found in the pristine flakes. The phonon dispersion $\omega(\mathbf{q})$ of 1L-MoS_2 is calculated using DFT. The region of $\omega(\mathbf{q})$ which is of interest for the E' and A'_1 peaks is shown in Fig. 2(a). At the $\mathbf{\Gamma}$ point, the out-of-plane optical (ZO) branch gives rise to the A'_1 mode. The slight polarity of MoS_2 breaks the degeneracy of the longitudinal optical (LO) and transverse optical (TO) branches at the zone center. However, due to the small LO-TO splitting ($<3\,\mathrm{cm}^{-1}$), only one peak, E', is detectable using Raman spectroscopy measurements [11,30].

From Eq. (1) we numerically calculate the line shapes of the A'_1 and E'_1 peaks (see Supplemental Material [31]), using the corresponding branches of the phonon dispersion curves. For the A'_1 peak, this is the dispersion of the ZO branch. Equation (1) is calculated for the LO and TO branches of the dispersion curve and then the sum of the two integrals is taken for the E' peak. We therefore assume that the LO and TO branches equally contribute to the line shape of the E' peak. The phonon branches giving rise to the A'_1 and E'_1 peaks are rigidly shifted by -6.6, -7.0, and $-9.7\,\mathrm{cm}^{-1}$ (for the ZO, TO, and LO branches, respectively), to match each $\mathbf{\Gamma}$-point value

to the experimental peak frequencies measured for pristine 1L-MoS_2. In the calculation the phonon correlation length is taken to be proportional to the interdefect distance [16], that is $L_C = \alpha L_D$, where α is a real, positive number.

Figures 2(c) and 2(d) show the experimental evolution of the position and linewidth of the E' and A_1' peaks as a function of L_D, calculated using Voigt peak fits as there are contributions from multiple peaks in this spectral range, as shown in Fig. 2(b). The upward and downward shifts of Pos(A_1') and Pos(E'), respectively, resemble the phonon dispersion of the corresponding branches: moving away from the $\mathbf{\Gamma}$ point ($\mathbf{q} \cong 0$), the upward trend for the ZO frequencies, and the downward trend for the LO and TO frequencies are observed. α is an adjustable factor, as the defect scattering cross sections are expected to be quite different for in-plane (E') and out-of-plane (A_1') modes. Here α is determined by achieving the best agreement with the experimental trends of Pos(E'), Pos(A_1'), $\Gamma(E')$, and $\Gamma(A_1')$. From Fig. 2 the optimal values for α are found to be 0.5 ± 0.1 and 0.8 ± 0.1 for the A_1' and E' peaks, respectively. Therefore, the phonon correlation length and the interdefect distance are of the same order of magnitude, supporting the validity of the proposed model. Note that these results are consistent with experiments on ion-bombarded graphene that show a proportionality between L_C and L_D, with different values of α associated with different modes [16].

Other than the effects of phonon confinement on the two first-order 1L-MoS_2 Raman peaks, the Raman spectra of the Mn^+ bombarded samples are also characterized by the presence of defect-activated peaks. The peak positions and relative assignments, based on the correlation with the theoretical phonon dispersion [Figs. 2(a) and 3(a)], are reported in Table I. These modes involve phonons at the zone edge of the Brillouin zone, which may be activated by the momentum contribution of a defect, allowing the Raman selection rule to be satisfied. Similar peaks have been previously reported in other transition metal dichalcogenides (TMDs) under electronic resonance condition, and ascribed to disorder-induced modes originated at the zone edge [32]. Some of these modes, while still clearly distinguishable, overlap with the E' and A_1' peaks, affecting the uncertainty in the fitting process.

For peaks in close proximity to the first-order peaks, the defect-induced peak at $\sim$357 cm^{-1} can be assigned to the TO branch at the **M** point, while at the high frequency side of the A_1' peak it is possible to distinguish a peak centered at

TABLE I. Disorder-activated Raman band position and respective assignment.

Band (cm^{-1})	Assignment
154.5 ± 2.4	TA(M)
180.6 ± 1.9	ZA(M)
187.9 ± 0.8	TA(K)
215.2 ± 2.0	–
227.6 ± 0.7	LA(M)[a]
250.4 ± 1.5	–
357.7 ± 2.8	TO(M)
377.0 ± 1.1	LO(M)
411.9 ± 1.2	ZO(M)

[a]Assignment from Ref. [40].

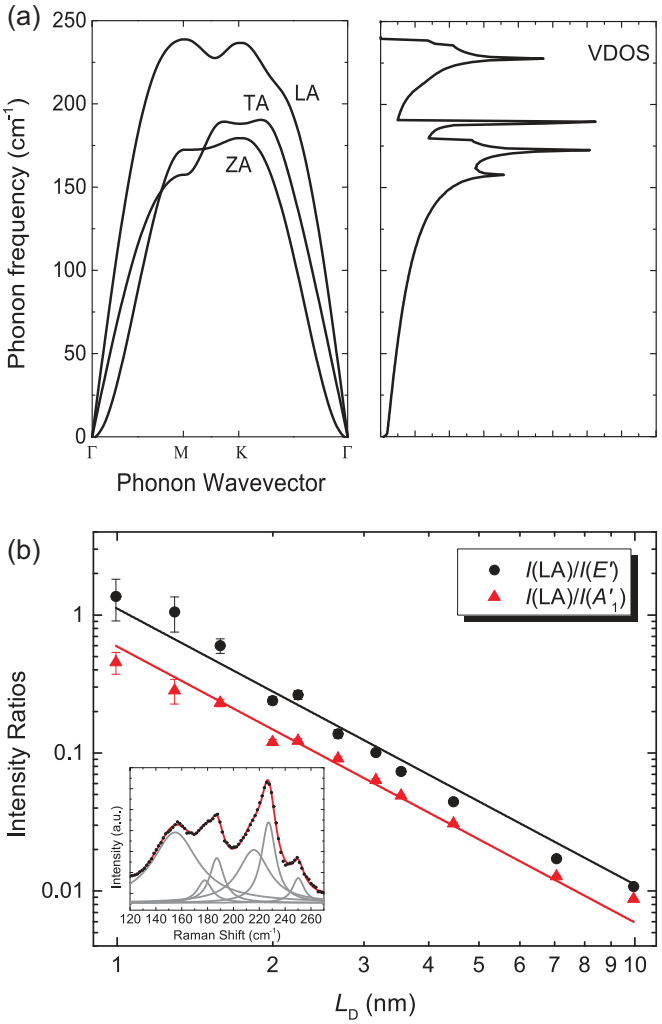

FIG. 3. (Color online) (a) Phonon dispersion and vibrational density of states of 1L-MoS_2. (b) Experimental intensity ratios $I(\mathrm{LA})/I(A_1')$ and $I(\mathrm{LA})/I(E')$ are reported in symbols. The error bars represent the standard error from the fitting process. The solid lines are linear fits with slope equal to -2. The low frequency bands, where the LA peak is located at $\sim$227 cm^{-1}, are shown in the inset, along with the corresponding Lorentzian fits.

$\sim$411 cm^{-1} that we assign to ZO(M). Of particular interest is the peak at $\sim$377 cm^{-1}, which overlaps with the E' peak until it becomes barely distinguishable for high levels of disorder. Indeed, the $\sim$377 cm^{-1} feature was previously identified not as a distinct peak, but as a broadening of the E' peak [9]. This is not the case, as clearly evidenced from the comparison between the spectra with different levels of disorder (Fig. 1). The distinctive identity of the $\sim$377 cm^{-1} peak is further confirmed by its presence in pristine 1L-MoS_2, where it manifests itself as a weak shoulder located at the low-frequency side of the E' peak. The existence of a similar shoulder has been previously reported for bulk MoS_2, and it has been assigned to Raman-inactive TO phonons with E^2_{1u} symmetry [33], arising from an atomic displacement pattern similar to that of E^1_{2g}. This assignment is questionable, as reflectivity measurements show this peak at the higher frequency side of the E' peak [34]. Moreover, the distinction between the E^1_{2g} and the E^2_{1u} modes

is not present in 1L-MoS_2 [35], where a single E' peak should be observed. Therefore, we consider that the origin of the low frequency shoulder cannot be attributed to E^2_{1u}. This study enables the $\sim$377 cm^{-1} feature to be identified as a disorder-induced peak, suggesting that it is a mode originated at the edge of the Brillouin zone [LO(M)].

Analyzing the low-frequency region of the Raman spectrum (140–260 cm^{-1}) of Mn^+ bombarded 1L-MoS_2 (see Fig. 1), we observe the appearance of new bands. Among these, the most intense peak is located at $\sim$227 cm^{-1}. It has previously been shown that exposure to ambient conditions can cause partial oxidation of MoS_2, and therefore leading to the presence of molybdenum oxides, with MoO_3 displaying Raman bands [36] in the spectral region 120–1110 cm^{-1}. The most prominent peak of MoO_3 is located at $\sim$820 cm^{-1} and is attributed to a symmetric stretch of the oxygen atoms in the O–Mo–O bond [36], while a very weak band is also present at $\sim$227 cm^{-1}. Therefore, one possible assignment of the $\sim$227 cm^{-1} peak in 1L-MoS_2 could be an increased level of partial oxidation on the MoS_2 samples, as vacancy sites are expected to interact with molecular oxygen, thus promoting the formation of Mo–O bonds. However, if this were the case, the onset of the MoO_3 band at $\sim$227 cm^{-1} should be accompanied by a distinct appearance of a much more intense peak at $\sim$820 cm^{-1}. In the Raman spectra of Mn^+ bombarded MoS_2, a peak is observed at $\sim$820 cm^{-1} but its intensity does not increase as a function of disorder, indicating that it corresponds to a higher order MoS_2 peak [37] (see Supplemental Material [38]).

A prominent peak at $\sim$227 cm^{-1} has also previously been reported in literature in deposited MoS_2 films [39] and MoS_2 nanoparticles [40]. Studying MoS_2 nanoparticles, Frey *et al.* [40] attributed the $\sim$227 cm^{-1} peak to disorder-induced Raman scattering. This peak has been linked to the presence of a local maximum in the vibrational density of states (VDOS), located at the energy corresponding to the longitudinal acoustic (LA) branch at the edge of the Brillouin zone [35] [Fig. 3(a)]. The emerging peak has been assigned to LA phonons with momentum $\mathbf{q} \neq 0$ at **M** point, and referred in literature as LA(M) [40], which is the term that will also be used from herein. However, restricting the origin of the peak to **M**-point phonons may not be completely justified, as (i) the VDOS presents a Van Hove singularity between the **M** and **K** point, and (ii) the LA branch is almost dispersionless over the entire edge of the Brillouin zone, that is, all the phonons at the zone edge have similar energies and could potentially contribute to the $\sim$227 cm^{-1} peak. The second order of LA(M) is also present in the spectra at $\sim$454 cm^{-1} and it is denoted as 2LA(M) (Fig. 1). The origin of this band is interesting and will also be discussed later.

To further validate the strong correlation between the $\sim$227 cm^{-1} peak and structural defects, the evolution of the intensity (peak height) of the LA(M) peak, normalized to the E' peak, $I(\mathrm{LA})/I(E')$, and the A'_1 peak, $I(\mathrm{LA})/I(A'_1)$, respectively, as a function of L_D is shown in Fig. 3(b). The increase of these intensity ratios is the combination of two concomitant factors occurring upon increasing disorder: (i) an increase in the absolute intensity of the $\sim$227 cm^{-1} peak, caused by the increase in disorder, and (ii) a decrease in the intensity of the E' and A'_1 peaks that is possibly due to the progressive ablation of the material caused by the ions bombarding the MoS_2 flakes. The latter is observed in Fig. 1 from the increase in the intensity of the Si peak, observed at $\sim$300 cm^{-1} and labeled with an asterisk, with decreasing L_D (note that the spectra in Fig. 1 are normalized to the A'_1 peak). On the basis of these observations, we show that $I(\mathrm{LA})/I(E')$ and $I(\mathrm{LA})/I(A'_1)$ are inversely proportional to L_D^2, or, equivalently, directly proportional to the total number of ions impinging on the surface ($1/L_D^2$). Fitting the data in Fig. 3(b) using

$$\frac{I\,(\mathrm{LA})}{I\,(X)} = \frac{C\,(X)}{{L_D}^2}, \tag{2}$$

where $X = E'$ or A'_1, reveals that $C(E') = 1.11 \pm 0.08\ nm^2$ and $C(A'_1) = 0.59 \pm 0.03\ nm^2$. These values are expected to be dependent on the laser excitation energy used for the Raman measurements. A similar relationship is found when using the frequency-integrated peak intensities (see Supplemental Material [41]). Interestingly, these intensity ratios behave analogously to the intensity ratio of the D and the G peak, $I(D)/I(G)$, in graphene, which is largely used to assess the level of disorder within the lattice [14–16].

Besides the prominent mode at $\sim$227 cm^{-1}, we can resolve other peaks in the region 140–260 cm^{-1}, whose intensities increase with disorder. Similarly to the $\sim$227 cm^{-1} peak, from Fig. 3(a), these bands appear to be linked to acoustic zone-edge phonons: we assign the peaks located at $\sim$154, $\sim$180, and $\sim$187 cm^{-1} to the TA(M), ZA(M), and TA(K) modes, respectively.

It is interesting to observe that, except for the peak at 187 cm^{-1}, all disorder-induced peaks in Table I match well with **M**-point phonons. The explanation for this preferential phonon activation within the Brillouin zone might be similar to the one suggested for the origin of the 2LA(M) band. Indeed, it has been recently shown that this band becomes more intense than the first-order A'_1 and E' peaks when the Raman experiment is performed with laser energies around 2 eV, which corresponds to the B-exciton energy in 1L-MoS_2 [42]. The mechanism proposed to account for this behavior is a double resonance (DR) process which involves two LA(M) phonons with opposite momentum. According to this model, originally used to explain the 2LA(M) band in tungsten disulfide (WS_2) [43], the Raman process involves resonances at valleys at the **K** and **I** points in the electronic band structure (the **I** point is the intermediate point between the **Γ** and **K** points) and the phonon which connects these two valleys has a wave vector at the **M** point. At the origin of the defect-induced peaks in 1L-MoS_2 there could be a similar DR process involving a single phonon mode at **M** and scattering due to defects for momentum conservation. This would be comparable to graphene, where the defect-induced D peak and the relative second-order 2D peak are activated by a DR process [44]. In order to check the validity of the DR mechanism in 1L-MoS_2, a resonance Raman study with varying laser excitation energy will be needed.

IV. CONCLUSIONS

In summary, we have investigated the effects of defects induced by Mn^+ ion bombardment on the Raman spectrum

of 1L-MoS_2. The degree of disorder is quantified by the interdefect distance L_D. The E' peak and the A_1' peak broaden upon increasing the defect density, which is accompanied by a downshift of the position of the E' peak and an upshift of the position of the A_1' peak. Using DFT calculations of the phonon dispersion, we have explained the evolution of these first-order peaks as due to phonon confinement. Moreover, the introduced disorder activates new Raman modes, many of which have not been observed in literature, and that we assign as arising from zone-edge phonons. Among these, we have focused attention on the $\sim 227\,cm^{-1}$ peak, which has been assigned to LA phonons at the **M** point. We have proposed a phenomenological relationship between the intensity ratio of the LA(M) peak and each of the first-order peaks, allowing a fast and practical quantification of defects in 1L-MoS_2 using Raman spectroscopy. Finally, the preferential activation of **M**-point phonons due to disorder has shed light on possible electronic resonance phenomena, which are likely to trigger a debate on the role of the electron-phonon coupling in the Raman scattering of 1L-MoS_2 and other two-dimensional TMDs.

ACKNOWLEDGMENTS

S.M., A.J.P., B.B., I.S.G., and D.R. acknowledge financial support from the Innovation Research and Development Programme of the National Measurement System, UK, Project No. 115948. N.B. acknowledges support from the EU Seventh Framework Programme through the MC-CIG Ref. 294158. The authors would also like to thank Steve J. Spencer for aid in preparation of the samples.

[1] A. K. Geim and I. V. Grigorieva, Nature (London) **499**, 419 (2013).
[2] K. F. Mak, C. Lee, J. Hone, J. Shan, and T. F. Heinz, Phys. Rev. Lett. **105**, 136805 (2010).
[3] B. Radisavljevic, A. Radenovic, J. Brivio, V. Giacometti, and A. Kis, Nat. Nanotechnol. **6**, 147 (2011).
[4] A. Splendiani, L. Sun, Y. Zhang, T. Li, J. Kim, C. Y. Chim, G. Galli, and F. Wang, Nano Lett. **10**, 1271 (2010).
[5] W. Zhou *et al.*, Nano Lett. **13**, 2615 (2013).
[6] H.-P. Komsa, J. Kotakoski, S. Kurasch, O. Lehtinen, U. Kaiser, and A. V. Krasheninnikov, Phys. Rev. Lett. **109**, 035503 (2012).
[7] S. Tongay *et al.*, Sci. Rep. **3**, 2657 (2013).
[8] J. Kibsgaard, Z. Chen, B. N. Reinecke, and T. F. Jaramillo, Nat. Mater. **11**, 963 (2012).
[9] Y. Liu *et al.*, ACS Nano **7**, 4202 (2013).
[10] B. Chakraborty, A. Bera, D. V. S. Muthu, S. Bhowmick, U. V. Waghmare, and A. K. Sood, Phys. Rev. B **85**, 161403(R) (2012).
[11] C. Rice, R. J. Young, R. Zan, U. Bangert, D. Wolverson, T. Georgiou, R. Jalil, and K. S. Novoselov, Phys. Rev. B **87**, 081307(R) (2013).
[12] C. Lee, H. Yan, L. E. Brus, T. F. Heinz, J. Hone, and S. Ryu, ACS Nano **4**, 2695 (2010).
[13] S. Jiménez Sandoval, D. Yang, R. F. Frindt, and J. C. Irwin, Phys. Rev. B **44**, 3955 (1991); X. Zhang, W. P. Han, J. B. Wu, S. Milana, Y. Lu, Q. Q. Li, A. C. Ferrari, and P. H. Tan, *ibid.* **87**, 115413 (2013).
[14] A. J. Pollard, B. Brennan, H. Stec, B. J. Tyler, M. P. Seah, I. S. Gilmore, and D. Roy, Appl. Phys. Lett. **105**, 253107 (2014).
[15] M. M. Lucchese, F. Stavale, E. H. M. Ferreira, C. Vilani, M. V. O. Moutinho, R. B. Capaz, C. A. Achete, and A. Jorio, Carbon **48**, 1592 (2010); L. G. Cançado *et al.*, Nano Lett. **11**, 3190 (2011).
[16] E. H. Martins Ferreira, M. V. O. Moutinho, F. Stavale, M. M. Lucchese, R. B. Capaz, C. A. Achete, and A. Jorio, Phys. Rev. B **82**, 125429 (2010).
[17] J. B. Park, C. B. France, and B. A. Parkinson, J. Vac. Sci. Technol. B **23**, 1532 (2005); A. Prodan, V. Marinkovic, R. Gril, N. Ramsak, H. J. P. van Midden, F. W. Boswell, and J. C. Bennett, *ibid.* **18**, 60 (2000).
[18] K. S. Novoselov, D. Jiang, F. Schedin, T. J. Booth, V. V. Khotkevich, S. V. Morozov, and A. K. Geim, Proc. Natl. Acad. Sci. USA **102**, 10451 (2005).
[19] P. Giannozzi *et al.*, J. Phys.: Condens. Matter **21**, 395502 (2009).
[20] J. P. Perdew and A. Zunger, Phys. Rev. B **23**, 5048 (1981).
[21] See Supplemental Material at http://link.aps.org/supplemental/10.1103/PhysRevB.91.195411 for the Raman spectra of defective 1L-MoS_2 as a function of laser power.
[22] A. H. Castro Neto, N. M. R. Peres, K. S. Novoselov, and A. K. Geim, Rev. Mod. Phys. **81**, 109 (2009).
[23] N. Blanc, F. Jean, A. V. Krasheninnikov, G. Renaud, and J. Coraux, Phys. Rev. Lett. **111**, 085501 (2013).
[24] E. Scalise, M. Houssa, G. Pourtois, V. V. Afanas′ev, and A. Stesmans, Physica E **56**, 416 (2014).
[25] E. Asari, I. Kamioka, K. G. Nakamura, T. Kawabe, W. A. Lewis, and M. Kitajima, Phys. Rev. B **49**, 1011 (1994).
[26] K. Ishioka, K. G. Nakamura, and M. Kitajima, Phys. Rev. B **52**, 2539 (1995).
[27] H. Richter, Z. P. Wang, and L. Ley, Solid State Commun. **39**, 625 (1981).
[28] I. H. Campbell and P. M. Fauchet, Solid State Commun. **58**, 739 (1986).
[29] S. Piscanec, M. Cantoro, A. C. Ferrari, J. A. Zapien, Y. Lifshitz, S. T. Lee, S. Hofmann, and J. Robertson, Phys. Rev. B **68**, 241312(R) (2003).
[30] H. J. Conley, B. Wang, J. I. Ziegler, R. F. Haglund, S. T. Pantelides, and K. I. Bolotin, Nano Lett. **13**, 3626 (2013).
[31] See Supplemental Material at http://link.aps.org/supplemental/10.1103/PhysRevB.91.195411 for the line shapes of the Raman scattering peaks (E' and A_1') calculated using the model described in the main text.
[32] E. Del Corro, H. Terrones, A. Elias, C. Fantini, S. Feng, M. A. Nguyen, T. E. Mallouk, M. Terrones, and M. A. Pimenta, ACS Nano **8**, 9629 (2014).
[33] T. Sekine, K. Uchinokura, T. Nakashizu, E. Matsuura, and R. Yoshizaki, J. Phys. Soc. Jpn. **53**, 811 (1984); T. Livneh and E. Sterer, Phys. Rev. B **81**, 195209 (2010).
[34] T. J. Wieting and J. L. Verble, Phys. Rev. B **3**, 4286 (1971).

[35] A. Molina-Sánchez and L. Wirtz, Phys. Rev. B **84**, 155413 (2011).

[36] B. C. Windom, W. G. Sawyer, and D. W. Hahn, Tribol. Lett. **42**, 301 (2011).

[37] J. M. Chen and C. S. Wang, Solid State Commun. **14**, 857 (1974); L. Sun *et al.*, Phys. Rev. Lett. **111**, 126801 (2013).

[38] See Supplemental Material at http://link.aps.org/supplemental/10.1103/PhysRevB.91.195411 for the high frequency region (700–850 cm^{-1}) of the Raman spectra as a function of L_D.

[39] N. T. McDevitt, J. S. Zabinski, M. S. Donley, and J. E. Bultman, Appl. Spectrosc. **48**, 733 (1994).

[40] G. L. Frey, R. Tenne, M. J. Matthews, M. S. Dresselhaus, and G. Dresselhaus, Phys. Rev. B **60**, 2883 (1999); J. Mater. Res. **13**, 2412 (1998).

[41] See Supplemental Material at http://link.aps.org/supplemental/10.1103/PhysRevB.91.195411 for the plot of the ratios of the experimental frequency-integrated peak intensities, $A(\mathrm{LA})/A(A_1')$ and $A(\mathrm{LA})/A(E')$, as a function of L_D.

[42] M. A. Pimenta, E. Del Corro, B. R. Carvalho, C. Fantini, and L. M. Malard, Acc. Chem. Res. **48**, 41 (2015)

[43] A. Berkdemir *et al.*, Sci. Rep. **3**, 1755 (2013).

[44] P. Venezuela, M. Lazzeri, and F. Mauri, Phys. Rev. B **84**, 035433 (2011).